Kinesin's Network of Chemomechanical Motor Cycles

Steffen Liepelt and Reinhard Lipowsky
Max Planck Institute of Colloids and Interfaces, Science Park Golm, 14424 Potsdam, Germany
(Received 8 December 2006; published 20 June 2007)

A general network theory for the molecular motor kinesin is developed that is based on the distinct chemical states of the motor and on recent observations about its mechanical steps. For small concentrations of adenosine diphosphate (ADP), the motor's behavior is governed by the competition of two chemomechanical motor cycles which determine the motor's stall force. A third cycle becomes important for large ADP concentrations. The theory provides a quantitative description for the functional dependencies of different motor properties as observed in single molecule experiments.

DOI: 10.1103/PhysRevLett.98.258102 PACS numbers: 87.16.Nn, 82.39.Fk, 87.16.Uv

Kinesin is a molecular motor [1,2] that walks processively on microtubules and is essential for intracellular transport and structure formation over many length and time scales [3]. Its motor properties have been determined in a long series of sophisticated experiments [4–16]. Its processive walks consist of about 100 steps and take a few seconds [4]. Each motor step consists of an 8-nm-displacement along the filament [5] via "hand-over-hand" movement of kinesin's two identical motor heads [13]. During each step, the motor hydrolyzes one adenosine triphosphate (ATP) molecule into one adenosine diphosphate (ADP) molecule and inorganic phosphate, P [7]. The released chemical energy then drives conformational transitions of the motor molecule and enables it to perform mechanical work.

As far as theory is concerned, a large number of different models has been discussed. Many of these models emphasized generic aspects and did not directly address specific experimental data, see, e.g., [17]. In a series of papers, Fisher and coworkers [18,19] developed discrete stochastic models that matched several sets of experimental data [9,11]. These latter models have, however, two important limitations. First, they are based on a single motor cycle for which the stall force is necessarily determined by the flux balance between ATP hydrolysis and ATP synthesis [19]. Since the ATP synthesis rate is proportional to ADP concentration, the latter balance would imply that the ATP hydrolysis rate vanishes at the stall force in the limit of small ADP concentration. Recent experiments provide, however, strong evidence that the ATP hydrolysis rate is finite in this limit [15]. Second, the models in [18,19] do not incorporate the energetics of ATP hydrolysis [20] and the associated steady state balance conditions [21] that replace the usual detailed balance conditions and provide important thermodynamic constraints on the transition rates.

In this Letter, we present a general network theory for the chemomechanical coupling of kinesin, see Fig. 1, that incorporates (i) several motor cycles and (ii) the steady state balance conditions for the transition rates. Our theory provides a unified description for several sets of experimental data, including two recent ones (i) by Carter and Cross [15], who provided evidence that the displacement of the kinesin motor involves only a single mechanical step without substeps and that the backward steps may involve ATP hydrolysis as well, and (ii) by Schief *et al.* [12], who found that the motor velocity decreases both with increasing P and increasing ADP concentration.

We start from a general description of the different chemical states of the two-headed motor. These states are connected by transitions corresponding to changes in chemical composition, e.g., ATP binding, P release, etc., We focus on the motor's processive motion for which the two motor heads are expected to be "out-of-phase." This

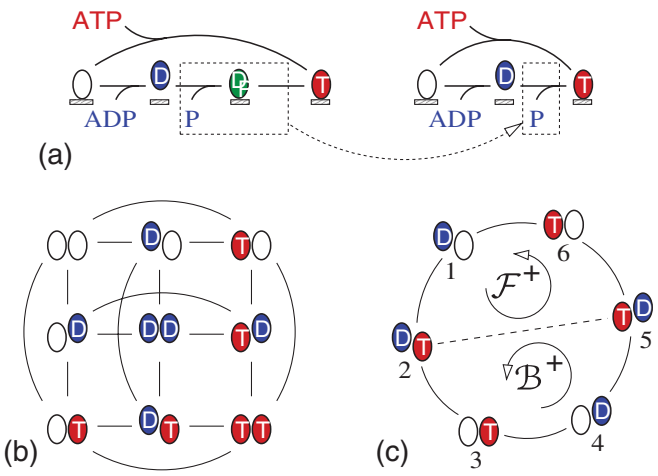

FIG. 1 (color). (a) Chemical cycle for a single motor head and its reduction to 3 states; (b) Kinesin state space consisting of $3^2 = 9$ chemical states and 18 chemical transitions (full lines) between these states; and (c) 6-state model obtained from (b) by omitting the three states *EE*, *DD* and *TT*. The six states $i = 1, 2, \ldots 6$ form a single chemical cycle, $\langle 1234561 \rangle$. The mechanical stepping transition $\langle 25 \rangle$ (broken line) divides this chemical cycle up into two chemomechanical cycles, $\mathcal{F}$ and $\mathcal{B}$, see text. Every line between two states i and j represents both the forward transition, $|ij\rangle$, from i to j and the backward transition, $|ji\rangle$, from j to i. As indicated by the vertical head displacements, the *E* and *T* states are strongly bound whereas the *D* state is weakly bound to the microtubule [6,16].

leads to a reduced state space of those 6 states in which the two heads have a different chemical composition. We then argue that the mechanical steps should connect only two of these states. The resulting 6-state model exhibits two chemomechanical motor cycles, one for the forward and one for the backward step. The flux balance between these two cycles, which both involve ATP hydrolysis, determines the stall force of the motor.

As shown below, the 6-state model provides a good description for almost all measured properties of kinesin's processive motion. There is one exception, however: the decrease of motor velocity with increasing ADP concentration, as calculated for the 6-state model, is not as fast as observed experimentally in [12]. In order to match the observed velocity/ADP relationship, we found it necessary to include another motor state in which both heads contain bound ADP. The resulting 7-state model contains a third chemomechanical motor cycle and provides a quantitative description for all measured properties of kinesin's processive motion as well as for its run length.

Kinesin's state space.—The rate of P release from a motor head is limited by the preceding hydrolysis rate, i.e., P is released immediately after ATP hydrolysis [14]. We therefore combine these two subsequent transitions into a single one as shown in Fig. 1(a). Each motor head can now be empty (E) and contain bound ATP (T) or ADP (D). Since the kinesin molecule has two motor heads, the state space contains $3^2 = 9$ states that differ in chemical composition, see Fig. 1(b).

The chemical kinetics of the two heads is coordinated: binding of ATP to one head leads to the release of ADP from the other head [8,14]. The tight coupling of ATP hydrolysis and stepping as well as the hand-over-hand movement indicate that such an out-of-phase behavior of the two heads also governs the catalytic action of stepping kinesin. We thus focus on those states in Fig. 1(b) for which the two heads have different chemical composition. In this way, we arrive at the reduced state space shown in Fig. 1(c).

6-state model.—During the *mechanical* step, the leading and the trailing head interchange their positions. Since Carter and Cross [15] found no evidence for mechanical substeps, we incorporate this step as a single transition into the chemical cycle in Fig. 1(c). In general, the forward step could correspond to the transitions $|63\rangle$, $|14\rangle$, or $|25\rangle$. However, the transition $|63\rangle$ can be ruled out since the trailing head should unbind from the D state. In addition, a mechanical transition $|14\rangle$ would lead to a reduction of the motor velocity at high ATP concentration since the ATP binding transition $|12\rangle$ would then compete with the mechanical transition $|14\rangle$. Since such a decrease of motor velocity with ATP concentration is not observed experimentally, we conclude that the mechanical forward and backward step correspond to the transition $|25\rangle$ and $|52\rangle$, respectively, see broken line in Fig. 1(c).

Inspection of Fig. 1(c) shows that the complete 6-state model contains six directed motor cycles or *dicycles*: $\mathcal{F}^+ \equiv |12561\rangle$, $\mathcal{B}^+ \equiv |45234\rangle$, $\mathcal{D}^+ \equiv |1234561\rangle$, and the corresponding reverse dicycles $\mathcal{F}^-$, $\mathcal{B}^-$, and $\mathcal{D}^-$. The chemomechanical dicycle $\mathcal{F}^+$ includes the ATP hydrolysis transition $|61\rangle$ and the forward stepping transition $|25\rangle$, whereas the chemomechanical dicycle $\mathcal{B}^+$ includes the ATP hydrolysis transition $|34\rangle$ and the backward stepping transition $|52\rangle$. During the dissipative dicycle $\mathcal{D}^+$, the motor hydrolyzes two ATP molecules without making any step whereas the dicycles $\mathcal{F}^-$, $\mathcal{B}^-$, and $\mathcal{D}^-$ involve the ATP synthesis transitions $|16\rangle$ and/or $|43\rangle$.

Motor dynamics.—At time t, the motor occupies state i with probability $P_i(t)$. This probability evolves according to the Master equation $\frac{d}{dt}P_i = -\sum_j \Delta J_{ij}$ with the local excess fluxes $\Delta J_{ij} \equiv P_i\omega_{ij} - P_j\omega_{ji}$ where the transition rates ω_{ij} are equal to the number of transitions $|ij\rangle$ per unit time. The transition rates ω_{ij} depend on the load force F as well as on the molar concentrations $[X]$ with $X =$ ATP, ADP, or P, and can be written as

$$\omega_{ij} \equiv \kappa_{ij}\mathcal{I}_{ij}([X])\Phi_{ij}(F) \quad \text{with} \quad \Phi_{ij}(F=0) \equiv 1 \qquad (1)$$

which defines the rate constants κ_{ij}, see App. A [22]. The functions $\mathcal{I}_{ij}([X]) \equiv 1$ unless the transition $|ij\rangle$ involves binding of the molecular species X. In the latter case, $\mathcal{I}_{ij}([X]) \equiv [X]$ as appropriate for dilute solutions.

The *steady state* of the motor is characterized by a time-independent probability distribution $P_i = P_i^{\mathrm{st}}$. In this case, each dicycle $\mathcal{C}^d$ with orientation $d = \pm$ carries a well-defined dicycle flux $J^{\mathrm{st}}(\mathcal{C}^d)$, and each cycle, $\mathcal{C}$, can be characterized by its steady state flux, $J^{\mathrm{st}}(\mathcal{C}) \equiv J^{\mathrm{st}}(\mathcal{C}^+) - J^{\mathrm{st}}(\mathcal{C}^-)$ [20]. Furthermore, all local excess currents $\Delta J_{ij} = \Delta J_{ij}^{\mathrm{st}}$ can be written as linear superpositions of these cycle fluxes. The motor velocity, e.g., is given by $v \equiv \ell\Delta J_{25}^{\mathrm{st}} = \ell[J^{\mathrm{st}}(\mathcal{F}) - J^{\mathrm{st}}(\mathcal{B})]$ with the step size $\ell = 8$ nm. Thus, in the 6-state model, this velocity is governed by the competition between the two motor cycles $\mathcal{F}$ and $\mathcal{B}$, and vanishes for $J^{\mathrm{st}}(\mathcal{F}) = J^{\mathrm{st}}(\mathcal{B})$ which determines the stall force. In the limit of small [ADP], the transition rates ω_{65} and ω_{32} vanish which implies that the dicycle fluxes $J^{\mathrm{st}}(\mathcal{F}^-)$ and $J^{\mathrm{st}}(\mathcal{B}^-)$ vanish as well. Thus, for small [ADP], the motor velocity is given by $v \approx \ell[J^{\mathrm{st}}(\mathcal{F}^+) - J^{\mathrm{st}}(\mathcal{B}^+)]$, and the stall force is determined by the two dicycles $\mathcal{F}^+$ and $\mathcal{B}^+$, which both involve ATP hydrolysis.

Balance conditions.—Because of constraints arising from nonequilibrium thermodynamics, the transition rates ω_{ij} must fulfill, for each dicycle $\mathcal{C}^d$, steady state balance conditions of the form [21]

$$k_BT \sum{}' \ln(\omega_{ij}/\omega_{ji}) = E_{\mathrm{ch}}(\mathcal{C}^d) - W_{\mathrm{me}}(\mathcal{C}^d), \qquad (2)$$

where the primed sum runs over all transitions $|ij\rangle$ contained in dicycle $\mathcal{C}^d$, see App. B [22]. The energy scale is provided by the thermal energy $k_BT = 4.1 \times 10^{-21}$ J at room temperature. The terms $E_{\mathrm{ch}}(\mathcal{C}^d)$ and $W_{\mathrm{me}}(\mathcal{C}^d)$ are the supplied chemical energy and the performed mechanical work, respectively, with $E_{\mathrm{ch}}(\mathcal{C}^-) = -E_{\mathrm{ch}}(\mathcal{C}^+)$ and $W_{\mathrm{me}}(\mathcal{C}^-) = -W_{\mathrm{me}}(\mathcal{C}^+)$.

The supplied chemical energy can be expressed in terms of the energy change $\Delta\mu$ that is obtained by adding one ATP to the system and releasing one ADP and one P from it. For dilute solutions, this difference is given by $\Delta\mu = k_B T \ln\{K_{\rm eq}[{\rm ATP}]/([{\rm ADP}][{\rm P}])\}$ with the equilibrium constant $K_{\rm eq} \simeq 4.9 \times 10^{11}\,\mu M$ [12]. For the different dicycles of the 6-state network in Fig. 1(c), one then has $E_{\rm ch}(\mathcal{F}^+) = E_{\rm ch}(\mathcal{B}^+) = \Delta\mu$ and $E_{\rm ch}(\mathcal{D}^+) = 2\Delta\mu$ as well as $W_{\rm me}(\mathcal{F}^+) = \ell F$, $W_{\rm me}(\mathcal{B}^+) = -\ell F$ and $W_{\rm me}(\mathcal{D}^+) = 0$. For $F = 0$, the steady state balance conditions (2) lead to the two relations

$$K_{\rm eq} = \frac{\kappa_{25}\kappa_{12}\kappa_{56}\kappa_{61}}{\kappa_{52}\kappa_{21}\kappa_{65}\kappa_{16}} = \frac{\kappa_{52}\kappa_{45}\kappa_{23}\kappa_{34}}{\kappa_{25}\kappa_{54}\kappa_{32}\kappa_{43}}, \qquad (3)$$

by which one can determine two rate constants in terms of the other rate constants and $K_{\rm eq}$.

For nonzero load force F, the balance conditions (2) lead to relations between the mechanical work and the force-dependent transition rate factors Φ_{ij} as introduced in (1). These relations can be *automatically* fulfilled by an appropriate choice of the factors Φ_{ij} as functions of the dimensionless force $\bar{F} \equiv \ell F/(k_B T)$. For the mechanical transitions $|25\rangle$ and $|52\rangle$, we take $\Phi_{25} \equiv \exp(-\theta\bar{F})$ and $\Phi_{52} \equiv \exp[(1-\theta)\bar{F}]$ with a load distribution factor θ as in [18]. For the force dependence of the chemical transitions, which describes the effects of mechanical strain on the catalytic motor domains, we take $\Phi_{ij} \equiv 2/\{1 + \exp[\chi_{ij}\bar{F}]\}$ with $\chi_{ij} = \chi_{ji}$. This parametrization incorporates the experimental observation [15] that there are no mechanical substeps, see App. C [22].

Specification of transition rates.—Using the experimental data in [8,9,12,15], the parameters of the transition rates ω_{ij} have been specified in a systematic way. The results for the rate constants κ_{ij} of the forward cycle $\mathcal{F}$ are displayed in Table I. For the backward cycle $\mathcal{B}$, all rate constants apart from κ_{54} were identified with the corresponding ones of $\mathcal{F}$. The balance condition (3) then implies $\kappa_{54} = (\kappa_{52}/\kappa_{25})^2\kappa_{21} \ll \kappa_{21}$. The load distribution factor θ was found to have the value $\theta = 0.65$ for the data in Refs. [15] and $\theta = 0.3$ for those in Ref. [9]. The parameters χ_{ij} have the values $\chi_{12} = 0.25$ and $\chi_{56} = \chi_{61} = 0.15$ for the data in [15] and $\chi_{12} = 0.25$ and $\chi_{56} = \chi_{61} = 0.05$ for data in [9].

Thus, the experimental data from different groups lead to slightly different values for the transition rate parameters. These differences may reflect (i) the different kinesin molecules used in these experiments which were prepared from squid optic lobe [9] or drosophila [12,15], and (ii) different ionic conditions used in the different motility assays. In Fig. 2, we show the force velocity relation for single kinesin molecules as described by the 6-state model and compare it with two different sets of data as obtained in [15] and in [9]. In these experiments, the concentrations of the hydrolysis products ADP and P were presumably rather small. In contrast, Schief *et al.* [12] measured the motor velocity as a function of [P] and [ADP] but for $F = 0$. The corresponding data are compared in Fig. 3(a) and 3(b) with the solid lines from the 6-state model, which provides a good description for the reduction of the velocity with increasing [P] but underestimates the velocity reduction as observed with increasing [ADP]. Within the 6-state model, the latter reduction arises from the backward transitions $|65\rangle$ since $\omega_{65} \sim [{\rm ADP}]$.

TABLE I. Specification of the rate constants κ_{ij} for the cycle $\mathcal{F}$ of the 6-state model in Fig. 1(c). The first, second, and third rows contain the numerical values that apply to the experimental data in [9,12,15] as displayed in Figs. 2(a)–2(d), 3(a), and 3(b), respectively. The superscripts † and ⋆ indicate that the corresponding rate constant was estimated from bulk kinetic measurements [8] and via the balance condition (3), respectively. All rate constants are in units of $1/{\rm s}$, except for κ_{12}, κ_{65}, and κ_{16}, which have units $1/(\mu M{\rm s})$.

Expt.	κ_{25}	κ_{52}	κ_{12}	$\kappa_{21}^{\dagger}$	$\kappa_{56} = \kappa_{61}$	$\kappa_{65}^{\star}$	κ_{16}
[15]	3×10^5	0.24	2.0	100	100	0.02	(0.02)
[9]	3×10^5	(0.24)	1.8	100	200	0.09	(0.02)
[12]	(3×10^5)	(0.24)	4.0	100	225	0.25	0.02

7-state model.—In order to describe the velocity/[ADP] relationship in a quantitative manner, we found it necessary to include the DD state with $i = 7$ into our network description, see App. D and Fig. 5 in [22]. Within the resulting 7-state model, the motor undergoes the additional ADP binding transition $|17\rangle$, which competes with the ATP

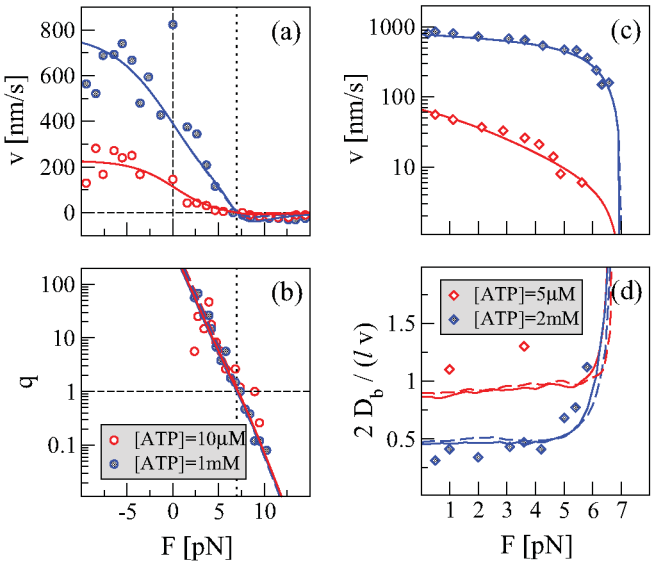

FIG. 2 (color). (a) Motor velocity v and (b) ratio q of the number of forward to backward steps as a function of external load force F (data from [15]). The ratio q has been calculated via $q = P_2\omega_{25}/(P_5\omega_{52})$. The vertical dotted line corresponds to the stall force F_s; (c) Motor velocity and (d) randomness parameter $2D_b/(\ell v)$ as a function of force F (data from [9]). The randomness is proportional to the bound state diffusion constant D_b. The solid and broken lines correspond to the 6- and 7-state model, respectively. In (a)–(c), the broken lines are (partially) masked by the solid lines.

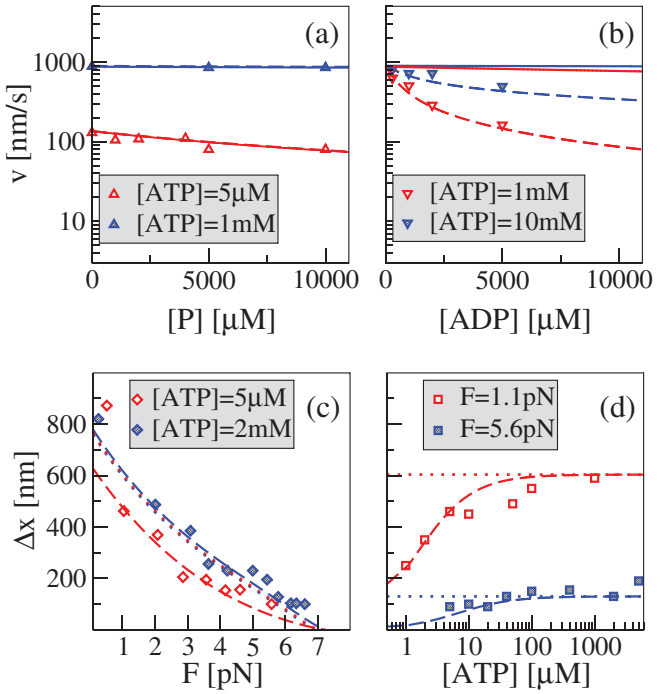

FIG. 3 (color). (a,b) Motor velocity v as a function of (a) P and (b) ADP concentration (data from [12]). The solid and broken lines are for the 6- and 7-state model, respectively; (c,d) Mean run length Δx as a function of (c) load force F and (d) ATP concentration (data from [10]). The broken and dotted lines correspond to the 7-state model with $[P] = [ADP] = 0.5\mu M$ and $[P] = [ADP] = 0\mu M$, respectively.

binding transition $|12\rangle$ and acts to reduce the motor velocity with increasing [ADP] as proposed in [12]. In this way, we also obtain a quantitative description of the velocity as a function of [ADP], see broken lines in Fig. 3(b). Calculation of the steady state fluxes reveals that, for large [ADP], the additional chemomechanical cycle $\langle 12571 \rangle$ becomes more important than the forward cycle $\langle 12561 \rangle$.

The 7-state model also enables us to calculate the average run length of kinesin which has been measured as a function of load force and [ATP] [10]. Since each head is expected to be weakly bound in the D state, the motor is most likely to unbind from the DD state. The average run length Δx is now obtained via $\Delta x = v/\epsilon_{ub} = v/P_7 \kappa_{70} \exp[\chi_{70} \bar{F}]$, where the unbinding rate ϵ_{ub} depends on the probability P_7 to be in the DD state, on the unbinding rate constant κ_{70}, and on the parameter χ_{70}. For $\kappa_{70} = 3.0/\mathrm{s}$ and $\chi_{70} = 0.1$, we obtain good agreement with the experimental data in [10], see Fig. 3.

Summary.—We have described a network theory for the chemomechanical coupling of the molecular motor kinesin that is based on the chemical state space of this motor and on the recent experimental observation [15] that its mechanical steps do not exhibit substeps. Our theory provides a quantitative description of the functional dependencies of motor velocity, ratio of forward to backward steps, and randomness parameter on the external control parameters as observed in single molecule experiments [9,10,12,15], see Figs. 2 and 3. One important aspect of our theory is the presence and competition of several chemomechanical motor cycles. For low [ADP], the motor properties are determined by the two cycles $\mathcal{F}$ and $\mathcal{B}$, see Fig. 1, which balance each other at the stall force. Therefore, one has to go beyond the usual unicycle models in order to understand the motor properties of kinesin. For large [ADP], yet another cycle becomes relevant that involves the weakly bound DD state. In order to further improve the transition rate estimates, it would be necessary to have a complete set of measurements for the same motility assay. Finally, our theory can be used to calculate additional motor properties such as the hydrolysis rate and the efficiency of the motor.

[1] M. Schliwa and G. Woehlke, Nature (London) **422**, 759 (2003).
[2] J. Howard, *Mechanics of Motor Proteins and the Cytoskeleton* (Sinauer, New York, 2001), 1st ed..
[3] R. Lipowsky and S. Klumpp, Physica A (Amsterdam) **352**, 53 (2005).
[4] S. M. Block, L. S. B. Goldstein, B. J. Schnapp, Nature (London) **348**, 348 (1990).
[5] K. Svoboda, C. F. Schmidt, B. J. Schnapp, and S. M. Block, Nature (London) **365**, 721 (1993).
[6] L. Romberg and R. Vale, Nature (London) **361**, 168 (1993).
[7] M. J. Schnitzer and S. M. Block, Nature (London) **388**, 386 (1997).
[8] S. P. Gilbert, L. M. Moyer, and K. A. Johnson, Biochemistry **37**, 792 (1998).
[9] K. Visscher, M. J. Schnitzer, and S. M. Block, Nature (London) **400**, 184 (1999).
[10] M. J. Schnitzer, K. Visscher, and S. M. Block, Nat. Cell Biol. **2**, 718 (2000).
[11] S. M. Block, C. L. Asbury, J. W. Shaevitz, and M. J. Lang, Proc. Natl. Acad. Sci. U.S.A. **100**, 2351 (2003).
[12] W. R. Schief, R. H. Clark, A. H. Crevenna, and J. Howard, Proc. Natl. Acad. Sci. U.S.A. **101**, 1183 (2004).
[13] A. Yildiz, M. Tomishige, R. D. Vale, and P. R. Selvin, Science **303**, 676 (2004).
[14] D. D. Hackney, Proc. Natl. Acad. Sci. U.S.A. **102**, 18338 (2005).
[15] N. J. Carter and R. A. Cross, Nature (London) **435**, 308 (2005).
[16] N. R. Guydosh and S. M. Block, Proc. Natl. Acad. Sci. U.S.A. **103**, 8054 (2006).
[17] R. Lipowsky, Phys. Rev. Lett. **85**, 4401 (2000).
[18] M. E. Fisher and A. B. Kolomeisky, Proc. Natl. Acad. Sci. U.S.A. **98**, 7748 (2001).
[19] M. E. Fisher and Y. C. Kim, Proc. Natl. Acad. Sci. U.S.A. **102**, 16209 (2005), and references therein.
[20] T. L. Hill, *Free Energy Transduction and Biochemical Cycle Kinetics* (Springer, New York, 1989).
[21] S. Liepelt and R. Lipowsky, Europhys. Lett. **77**, 50002 (2007).
[22] EPAPS document No. E-PRLTAO-98-020724. For more information on EPAPS, see http://www.aip.org/pubservs/epaps.html.